IEEE Access
Multidisciplinary | Rapid Review | Open Access Journal

IEEE VEHICULAR TECHNOLOGY SOCIETY SECTION

Received 23 June 2025, accepted 22 July 2025, date of publication 4 August 2025, date of current version 5 September 2025.

Digital Object Identifier 10.1109/ACCESS.2025.3595282

RESEARCH ARTICLE

Combining Model-Based and Data-Driven Observer Designs for Sideslip Angle Estimation

MARTIN REPKA[1], ALEXANDER L. GRATZER[2], (Member, IEEE), JAN FOJTASEK[1], TOMAS STRAKA[1], PETR PORTES[1], AND ALEXANDER SCHIRRER[2]

[1]Institute of Automotive Engineering, Brno University of Technology, 616 69 Brno, Czech Republic
[2]Institute of Mechanics and Mechatronics, TU Wien, 1060 Vienna, Austria

Corresponding author: Martin Repka (martin.repka1@vutbr.cz)

This work was supported by the Faculty of Mechanical Engineering, Brno University of Technology (BUT), under Grant FSI–S-23-8235.

ABSTRACT The vehicle side slip angle represents a key indicator of dynamic stability. Elevated values of the side slip angle may indicate a loss of stability or undesired vehicle behaviors such as understeering or oversteering. With the increased use of advanced driver assistance systems (ADAS), the need for accurate estimation of the side slip angle has become increasingly critical. This quantity in general needs to be indirectly measured or estimated, with the latter often representing a more cost-effective and more reliable approach. This is usually done by simple observer design, e.g., Kalman filter, which requires a well-parameterized system dynamics model. In this work we explore Machine Learning techniques in combination with a budget hardware inertial measurement unit to estimate the sideslip angle. This is done independently of the actual vehicle configuration, i.e., vehicle load and tires used. We model the system dynamics with a traditional Luenberger Observer, Long-short-term memory, Gated recurrent unit neural networks, and their combination, and investigate possible performance benefits when incorporating well-known physical relations. The results demonstrate that a well-designed combination of model-based and data-driven approaches can achieve high estimation accuracy even without the need for large datasets, which are typically required when employing purely data-driven methods. The performance of the proposed sideslip angle estimator under different driving conditions and tire configurations is validated with real-world measurement data.

INDEX TERMS Sideslip angle estimation, observer design, recurrent neural network, artificial neural network, physics-informed neural network, physics-infused neural network, hybrid observer design.

I. INTRODUCTION

Accurate vehicle dynamics models are crucial for the development and testing of modern control algorithms for safe and efficient automated and semi-automated driving on public roads [1], [2]. Vehicle dynamics play a pivotal role in ensuring the reliability and performance of the used prediction and control models. The vehicle sideslip angle β is a critical parameter in vehicle dynamics, particularly for assessing tire slips and overall vehicle stability during dynamic maneuvers. It can be measured using highly sophisticated and expensive methods, as discussed by Li et al. [3]. Alongside the yaw velocity (ω_z), β serves as a crucial indicator of vehicle stability [4], [5]. The longitudinal and lateral slips of the vehicle tires are essential criteria for evaluating the interaction between the road surface and tires [6]. However, direct measurement of β is often too expensive for regular road applications [7]. To that end, β is typically estimated utilizing model-based or data-driven approaches. Although model-based observers often struggle under varying or unknown external conditions [8], data-driven approaches, such as machine learning [9] or regression techniques [10], can address these challenges, provided that the encountered scenarios are sufficiently similar to portions of the training data used [8].

Estimating β presents challenges due to the non-linear dynamics of vehicle motion, which often limit the effectiveness of purely model-based methods. In contrast, data-driven

The associate editor coordinating the review of this manuscript and approving it for publication was Minh C. Ta.

machine learning techniques require extensive datasets that are not always readily available, particularly for the diverse driving conditions needed for accurate estimation. Consequently, a hybrid approach that combines model-based and data-driven methods can offer a more robust solution.

The overarching objective of this work is to obtain estimation results for β comparable to those obtained by the use of high-quality inertial measurement units (IMUs), which currently use ''Kalman Filter'' model-based observers, by leveraging low-budget IMUs, with limited sensor accuracy, which are currently deployed in vehicles for fleet testing.

A. RELATED WORK

The first application of neural networks for the β estimation was introduced by Kato et al. [9], where β is modelled as the sum of an approximate analytical expression and a corrective term from an artificial neural network. Inputs included the steering angle δ_{steer}, longitudinal a_x and lateral a_y accelerations, velocity $\dot{x}$, and yaw velocity ω_z. This approach demonstrated the feasibility of combining analytical and data-driven models for β estimation. Sasaki and Nishimaki [11] used a multi-layer neural network with ω_z and a_y as inputs for direct β estimation. Validated on a double lane-change maneuver, Sasaki's model highlighted that a simplified input set could still achieve accurate β estimation, showing that neural networks can model vehicle dynamics with minimal system knowledge. Melzi and Sabbioni [7] tested a feed-forward neural network with a single hidden layer on a simulated 7-degree-of-freedom (DOF) model in Simulink. This model described the center of gravity (COG) motion and provided inputs included $\dot{x}$, a_y, a_x, ω_z, and steering wheel angle δ_{steer}. The model also generated β output related to the COG motion, which was analyzed in the work. The study found satisfactory results but noted drift under low-excitation conditions, recommending a varied training dataset for optimal performance. Tristano et al. [4] compared the direct estimation of the β by an artificial neural network (ANN) to a physics-infused estimate that modelled β as a sum of dynamic and kinematic components. A sensitivity study showed that a simpler input set, using only the δ_{steer} and the a_y, improved generalization. This approach underscored the importance of minimizing input variables to avoid overfitting. Du et al. [12] developed a model with a prediction horizon of 0.5 s, using inputs such as wheel speed sensors ω_{fl}, ω_{fr}, ω_{rl}, ω_{rr}, yaw velocity ω_z, lateral acceleration a_y, and steering velocity $\dot{\delta}_{\text{steer}}$. Simulation results yielded a small average error, confirming the ANN's effectiveness for both estimation and predictive tasks in β applications. Chindamo and Gadola [13] used a black-box neural network trained with data from a Multibody simulation (MBS) software CarSim Simulator [14] under various conditions. Although adding neurons increased computation time, it did not improve accuracy, with optimal results achieved using a simple 5-10-1 architecture. This work highlighted that more complex networks do not necessarily enhance prediction accuracy. Gräber et al. [15] combined a Recurrent neural network (RNN) with a simplified 6-DOF kinematic model for estimating β. By providing $\dot{\beta} = \frac{a_y}{\dot{x}} - \omega_z$ to the gated recurrent unit (GRU) layer, they achieved better accuracy compared to the ''Kalman Filter'' based estimator across dry, wet, and snowy surfaces, showing the benefits of hybrid models. Sieberg and Novi explored combining an Unscented Kalman Filter (UKF) with an ANN for β [8], [16] and body roll angle ϕ_x [17] estimation. With a focus on embedded hardware constraints, they opted for simpler architectures with fewer neurons and a hyperbolic tangent transfer function. Their approach demonstrated effective implementation on limited hardware. Essa et al. [18] compared Feedforward neural network (FFNN), RNN, Long short-term memory (LSTM), and GRU for β estimation in IPG CarMaker. While FFNN achieved the highest accuracy, GRU provided the fastest solution, and LSTM offered a balance between accuracy and computational load. This study highlighted the trade-offs among different neural network architectures for the sideslip angle estimation. In their study, Bertipaglia et al. [19] demonstrate that a data-driven approach can achieve higher accuracy than a model-based approach, provided that sufficient quality data is available. The authors employ a Convolutional Neural Network (CNN) instead of an RNN for β estimation, with weights between the UKF and the Neural Network (NN) adjusted based on lateral acceleration. However, they note that deep NNs are prone to overfitting and lack generalization capabilities. While data-driven methods cannot guarantee robust performance across varying operating conditions, model-based approaches, despite their lower accuracy, offer consistent performance within the working region. The authors utilize a neural network architecture with two hidden layers (250 and 125 neurons), Rectified Linear Unit (ReLU) activation functions, a dropout rate of 0.2, and a learning rate of 0.001. They highlight that a slalom maneuver is particularly beneficial for testing, as it presents numerous challenging sideslip angle peaks. Ultimately, the authors conclude that with a limited dataset, the hybrid approach offers only a minor improvement in estimation accuracy over state-of-the-art Kalman Filter (KF) methods.

B. RESEARCH GAP AND CONTRIBUTION

Previous studies have explored the estimation of the vehicle sideslip angle using various approaches, including black-box ANNs [11], [18], physics-informed ANNs [8], [15], [16] (where the vehicle physical, or observer model provides the ANN with guidance on an approximate value of β), and physics-infused ANNs [4], [9] (where the ANN estimates only the difference between the physical, or observer model and the reference signal (ground truth)). These studies primarily focused on immediate β estimation using low-powered IMUs. Essa et al. [18] demonstrated different ANN architectures but treated the vehicle as a black-box. Gräber et al. [15] demonstrated the use of a physics-informed GRU

ANN, achieving satisfactory results based on measured data across different surfaces and tire sets.

Existing research has dedicated significant resources to constructing comprehensive datasets encompassing a wide spectrum of driving conditions for the estimation of β. The associated data acquisition process is often time-consuming and expensive. This raises the question: Can a data-driven estimator achieve accurate sideslip angle estimation using only datasets collected under typical, rather than extreme, driving conditions, thereby offering a more efficient and practical approach? Additionally, this work seeks to evaluate the adaptability of different prediction model structures to changes in system parameters, such as different tire sets, to enhance the robustness and accuracy of the sideslip angle estimation.

The following main contributions are developed hereafter:

1) A novel hybrid estimation structure, combining data-driven and model-based approaches, is developed and evaluated.
2) A comprehensive comparative analysis of LSTM and GRU estimators is conducted, utilizing real-world measurement data to assess their respective strengths and weaknesses.
3) The performance of the proposed algorithms is assessed through empirical evaluation, including field testing and real-world validation scenarios. The robustness of the developed estimator is demonstrated through evaluation on data acquired from a low-fidelity IMU employed in fleet testing.

C. PAPER OUTLINE

The remainder of this work is organized as follows: Section II delineates the problem formulation, including the experimental setup. Section III presents the proposed observer architectures for the estimation of the sideslip angle β. The obtained results are discussed in Section IV, while Section V concludes this paper.

II. PROBLEM FORMULATION

This section defines the observer design goals and describes the measurement vehicle, including its sensor configuration, utilized for data acquisition, testing, and validation. Following this, a physical vehicle model used for model-based observer design is presented. Finally, the dataset, used for training, validation, and evaluation, is described.

A. DESIGN GOALS

The main goal of this work is to develop accurate and versatile observers for the estimation of the difficult-to-measure sideslip angle β. This should be achieved by utilizing model-based, data-driven, and combined approaches. The training of the data-driven approaches should be based on real-world measurement data collected under typical rather than extreme driving conditions. The developed (hybrid) observers should offer more efficient, cost-effective, and practical tools for the estimation of β, also when combined with low-cost measurement devices – therefore democratizing sideslip angle estimation for a wide range of applications.

Additionally, to enhance the robustness and accuracy of the sideslip angle estimation, the adaptability of different observer designs to changes in the observed system's parameters, such as different tire sets, is investigated.

B. MEASUREMENT VEHICLE

The system under consideration is a front-wheel-steered multi-purpose road vehicle, a real instrumented measurement vehicle used at the Brno University of Technology, portrayed in Figure 1. Its relevant measured parameters are given in Table 1.

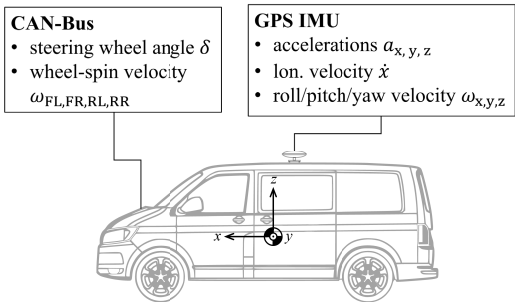

FIGURE 1. Measurement vehicle and sensor setup incl. vehicle-fixed coordinate frame.

TABLE 1. Measurement vehicle parameters.

m	3048	kg	Vehicle mass
L	3000	mm	Wheelbase
a	1433	mm	Hor. dist. from COG to front axle
b	1567	mm	Hor. dist. from COG to rear axle
h	550	mm	Vert. dist. from COG to axle plane
w_f	1628	mm	Track width front
w_r	1628	mm	Track width rear
J_z	6747	kg m^2	Moment of Inertia along z-axis
$F_{z,nom}$	7100	N	Nominal tire load

1) MEASUREMENT SETUP/SENSOR CONFIGURATION

The instrumentation/measurement setup comprised an NI cDAQ-9139 datalogger equipped with two NI-9862 high speed Controller Area Network (CAN) Flexible Data-rate (FD) interfaces, one for logging signals from the IMU and the other for data from the vehicle's standard sensors (such as steering wheel angle and wheel speed sensors) connected through onboard CAN-Bus and a low-budget IMU commonly used in vehicle fleet testing. A sampling rate of 100 Hz was employed, with the signal subsequently filtered using a Butterworth low-pass filter with a cutoff frequency of 5 Hz. This was then resampled to 10 Hz for the purposes of data analysis, evaluation and machine learning, in accordance with the procedures set out in ISO 15037-1 [20] for vehicle dynamics test methods. As in the approach described in [15], the IMU installed in the vehicle was a Genesys

ADMA-G-Pro+. This sensor can combine GPS and full IMU data (from 3 MEMS accelerometers and 3 closed-loop fibre optic gyroscopes) using built-in Kalman filters to determine the β, which, according to the manufacturer, has an RMS estimation error bound of 0.05° [21]. The low-budget IMU employed in this study integrates Micro-Electro-Mechanical Systems (MEMS) accelerometers, gyroscopes, and a GPS receiver. Data was acquired at a sampling frequency of 10 Hz and stored on an external flash drive. Subsequent post-processing, performed within the MATLAB environment, involved synchronization with data from a high-quality IMU [21]. For describing the forces and accelerations acting on the vehicle, the vehicle coordinate system defined in ISO 8855:2011(E) [22] is adopted. In this paper, the very accurate signals estimated by the IMU: the sideslip angle, with other signals from the high-quality ADMA IMU's accelerometers (a_x, a_y, a_z) and gyroscopes (ω_x, ω_y, ω_z), are considered as reference (ground truth). Data regarding δ_{steer} and ω_{fl}, ω_{fr}, ω_{rl}, ω_{rr} were gathered from the vehicle's CAN-Bus via the aforementioned measurement setup as is portrayed in Figure 1.

2) MEASUREMENT DATA COLLECTED

Out of the several hundred measurement channels available through the sensor configuration described in Section II-B1, the following subset of measurements will be used for the design of data-driven observers and validation purposes

$$\mathcal{M} = \left\{\delta_{\text{steer}}, \dot{x}, a_x, a_y, a_z, \omega_x, \omega_y, \omega_z, \omega_{\text{fl}}, \omega_{\text{fr}}, \omega_{\text{rl}}, \omega_{\text{rr}}\right\}, \tag{1}$$

where δ_{steer} denotes the steering wheel angle, $\dot{x}$ the longitudinal velocity of the vehicle, $a_{x,y,z}$ the longitudinal, lateral, and vertical acceleration, respectively, $\omega_{x,y,z}$ represents the pitch, roll and yaw velocities and $\omega_{\text{fl,fr,rl,rr}}$ represent the respective wheel speeds.

C. VEHICLE MODEL

As discussed in Section II-A, we will develop and investigate data-driven, model-based, and combined (hybrid) observer designs. Any model-based observer design necessitates a mathematical model of the system under investigation. To this end, in this section, the corresponding model of the measurement vehicle (compare Section II-B) is presented and described in detail.

We approximate the dynamics of the measurement vehicle with the widely used dynamic single-track vehicle model [23], a common simplification that treats wheels on a shared axle as a single wheel, thereby yielding a bicycle-like abstraction of the vehicle dynamics.

Even though the actual measurement vehicle is front-wheel steered, in this work, we utilize the dynamic single-track vehicle model with steerable front (δ_f) and rear axles (δ_r) in combination with a Luenberger-type observer to increase estimation accuracy for a broader operation range. Here, δ_r acts as a correction factor for the absence of elastokinematics (vehicle suspension kinematics, incorporating component compliance) and bump steer (tendency of a vehicle's wheels to steer themselves as the suspension moves vertically without any input from the steering [24]) in the 3-DOF single-track vehicle model. Details are given in Section III.

1) DYNAMIC SINGLE-TRACK VEHICLE MODEL

As part of the extended single-track vehicle observer, the dynamic single-track vehicle model with front- and rear-wheel steering is used to approximate the planar rigid body dynamics of the test vehicle. Specifically, we use the MATLAB/Simulink "Vehicle Body 3-DOF" library model with the external longitudinal velocity mode selected [25] to facilitate observer design and analysis, see Figure 2. A linear tire model is utilized that considers the lateral force via $F_y = C_\alpha \alpha$, compare [23]. The three DOFs of the model are the planar vehicle positions with respect to a global reference frame X and Y, and the yaw angle ψ described with respect to a vehicle-fixed coordinate frame located in the vehicle's centre of gravity (COG), compare Figure 2. The model is based on the assumption of quasi-steady-state longitudinal motion ($\ddot{x} = 0$) and yields sufficiently accurate results within the region of operation of lateral accelerations $a_y \leq 0.4\,\text{g}$ [26].

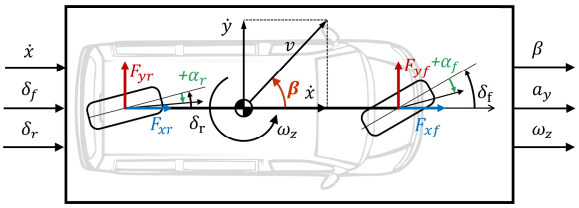

FIGURE 2. Dynamic single-track vehicle model with front- and rear-wheel steering.

The equations of motion are formulated as (cf. [23], [25])

$$\ddot{y} = -\dot{x}\,\omega_z + \frac{F_{y,f} + F_{y,r}}{m}, \tag{2a}$$

$$\dot{\omega}_z = \frac{a\,F_{y,f} - b\,F_{y,r}}{J_z}, \tag{2b}$$

with the yaw rate ω_z and the planar displacements with $a_y = \ddot{y} + \dot{x}\omega_z$ and $a_x = \ddot{x} - \dot{y}\omega_z$. The longitudinal and lateral tire forces acting on the front and rear axle, $F_{i,j}$ with $i \in \{x, y\}$ and $j \in \{f, r\}$, are described via

$$F_{x,f} = C_{\alpha_f}\alpha_f\,\mu_f\,\frac{F_{z,f}}{F_{z,\text{nom}}}\,\sin\left(\delta_f\right), \tag{3a}$$

$$F_{x,r} = C_{\alpha_r}\alpha_r\,\mu_r\,\frac{F_{z,r}}{F_{z,\text{nom}}}\,\sin\left(\delta_r\right), \tag{3b}$$

$$F_{y,f} = -C_{\alpha_\text{f}}\alpha_f\,\mu_f\,\frac{F_{z,f}}{F_{z,\text{nom}}}\,\cos\left(\delta_f\right), \tag{3c}$$

$$F_{y,r} = -C_{\alpha_\text{r}}\alpha_r\,\mu_r\,\frac{F_{z,r}}{F_{z,\text{nom}}}\,\cos\left(\delta_r\right), \tag{3d}$$

$$F_{z,f} = \frac{b\,m\,g - (\ddot{x} - \dot{y}\,\omega_z)\,m\,h}{a+b}, \tag{3e}$$

$$F_{z,r} = \frac{a\,m\,g - (\ddot{x} - \dot{y}\,\omega_z)\,m\,h}{a+b}, \tag{3f}$$

where $C_{\alpha \mathrm{f/r}}$ denotes the cornering stiffness of the front and rear axles, $\mu_{\mathrm{f/r}} = 1$ the friction coefficient, F_z the vertical force applied on the axles (aerodynamic axle lift forces were omitted), $\delta_{f/r}$ the steering angle of the front and rear axles and $\alpha_{\mathrm{f/r}}$ denotes the sideslip angle of the front and rear axles:

$$\alpha_f = \arctan\left(\frac{\dot{y} + a\omega_z}{\dot{x}}\right) - \delta_f \,, \tag{4a}$$

$$\alpha_r = \arctan\left(\frac{\dot{y} - b\omega_z}{\dot{x}}\right) - \delta_r \,, \tag{4b}$$

The formulation of Equations (3a)-(3d) employs a simplified linear tire model, wherein pure longitudinal and lateral slip are considered independently. The rationale of this independent use is illustrated in Fig 3, which presents normalized characteristic curves (measured in the laboratory) for one of the tire sets employed in this study (vertical axis scaled due to confidentiality), with multiple longitudinal slip (S_X) conditions. Quantitatively, a state with $S_X = 2\%$ exhibits a 2.45% difference in the cornering stiffness compared to a state with $S_X = 0\%$ (pure lateral slip). A total of 96.5 % of the measurement data obtained in this study corresponds to longitudinal slip values up to ± 2 %.

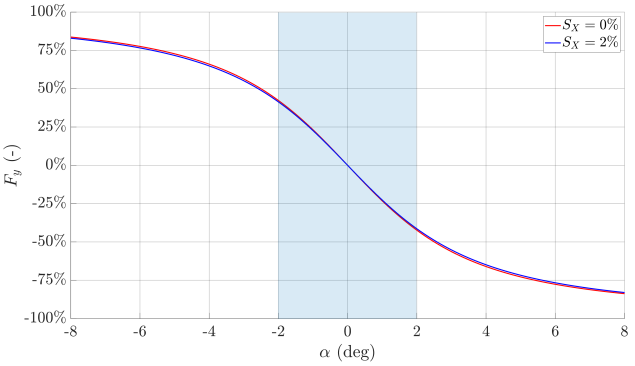

FIGURE 3. Comparison of tire lateral force characteristics for 0% and 2% longitudinal slip conditions. Relevant working area is highlighted in blue. The vertical axis is scaled due to confidentiality.

The sideslip angle can now be expressed in radians as a function of the longitudinal and lateral velocity (cf. [15]) by

$$\beta = \arctan\left(\frac{\dot{y}}{\dot{x}}\right) . \tag{5}$$

Based on the provided inputs $\boldsymbol{u} = \left[\dot{x}, \delta_f, \delta_r\right]^{\mathrm{T}}$, the dynamic single-track vehicle model calculates the desired outputs $\boldsymbol{y} = \left[\beta, a_y, \omega_z\right]^{\mathrm{T}}$, of which β is the most important one.

D. REAL-WORLD MEASUREMENT DATA COLLECTION

For the efficient training of the ANNs developed in the context of this work, we select the training data based on the recommendations from [7], which can be summarized as:

R1) The network should be trained with both clockwise and anti-clockwise maneuvers to prevent asymmetrical output behaviour.
R2) At least two different friction conditions should be considered in the training set.
R3) Maneuvers carried out at different speeds should be included.
R4) At least one maneuver with a significant longitudinal acceleration should be included in the training set.

In order to address points R1) and R3), the driving course was designed to incorporate a variety of surfaces and driving scenarios, including highways, country roads, dynamic driving, and calm driving. To address points R2) and R4), a speed profile with high longitudinal acceleration, ranging from $-5.3\,\mathrm{m\,s^{-2}}$ to $4.3\,\mathrm{m\,s^{-2}}$, was selected with longitudinal velocity reaching up to $145\,\mathrm{km\,h^{-1}}$. As implied by [15], acquiring data with small β values is relatively straightforward, whereas achieving large β values presents a considerable challenge. To ensure input features are on a comparable scale, thereby reducing training time and improving stability, Z-score normalization was applied to the data prior to training. The Z-score normalization was performed using the following formula:

$$x' = \frac{x - \mu}{\sigma} \,, \tag{6}$$

where x' denotes the normalized value, x the original value, μ denotes the mean, and σ represents the standard deviation. The test course, depicted in Figure 4, encompasses a total driving duration of 75 076 s and driven distance of 2918 km. In total, 5 different tire sets have been used. Training and validation utilized tiresets 1. and 2., covering two driving conditions for dry and wet surfaces with wet dataset forming approximately 30% of the training data set. Model performance was assessed using different tiresets, labeled 3., 4., and 5. as detailed in Table 2. Tiresets 3. and 4. have identical construction but differ in material, while tiresets 4. and 5. share the material but differ in construction. Due to confidentiality constraints, the cornering stiffness of the tiresets in Table 2 was normalized with tire set 2., exhibiting the highest cornering stiffness, set to 100%, and expressed as percentages.

TABLE 2. Tire sets used for real-world data collection.

Usecase	Tire set	C_α
Training	1.	93 %
Training + Validation	2.	100 %
Testing I.	3.	96 %
Testing II.	4.	90 %
Testing III.	5.	75 %

The evaluated dataset is visualized in Figure 4 and is divided into training, validation, and testing sets with an 80/11/9 ratio, respectively. 80 % of the acquired data, indicated by the blue line in Figure 4, was used for model training. 11% of the data, shown as the red-dashed line in Figure 4, was used for model cross-validation during the training process. This validation was conducted using tire set 2., as detailed

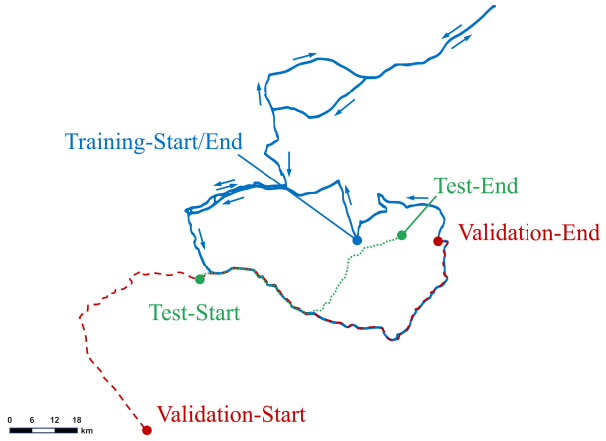

FIGURE 4. Test course: Training (blue), validation (dashed red), testing (dotted green).

in Table 2. Finally, 9% of the data, represented by the green-dotted line in Figure 4, was reserved for post-training model testing. This testing utilized tire sets 3.-5., as specified in Table 2.

III. PROPOSED OBSERVER ARCHITECTURES

As documented in [15] and [19], the accuracy of model-based observers depends significantly on the quality of the employed system designs used to estimate the states of the real vehicle. In contrast, the effectiveness of black-box data-driven methods depends heavily on the quality and diversity of the training data used. To overcome the limitations associated with both of these methodologies and to construct a model capable of accurately estimating β in both small and large β regimes, three hybrid approaches were developed: the physics-informed design (O3), the physics-infused design (O4) and their combination (O5). These designs integrate the strengths of model-based and data-driven techniques. For comparison, five distinct observer designs that span the spectrum of estimation strategies are evaluated: a purely model-based method (O1), a fully data-driven method (O2), and three hybrid designs (O3-O5).

DATA-DRIVEN ESTIMATOR DESIGN

As shown by [5], [7], and [27], ANNs can effectively model vehicle dynamics without requiring detailed knowledge of vehicle parameters, provided that an appropriate model structure and a sufficiently rich and diverse training dataset are used. This process is generally performed using heuristic approaches, as done in this work. When designing a neural network, three primary challenges are often encountered [8], [28]:

1) The number of neurons is too small, the network is unable to learn complex relationships in the data, and thus is not able to accurately model the data.
2) The network overfits the training data. When the number of neurons exceeds an optimal threshold, the network exhibits overfitting, characterized by a minimal training error and a degradation in performance when evaluated with new data.
3) The deployed network exhibits poor extrapolation capabilities. The nature of neural networks, as nonlinear Blackbox models, results in limited extrapolation abilities when deployed. Consequently, predictions for inputs outside the training data range are often unreliable.

MODEL-BASED OBSERVER (O1)

The first observer design is purely model-based and utilizes an extension of the dynamic single-track vehicle model described in Section II-C1. The observer is depicted in Figure 5. To enhance estimation accuracy, a Luenberger-type observer (LO) is implemented with the feedback gains G_1 and G_2 determined by the Simulink Parameter Estimator Toolbox [29] using the least squares optimization. The measured steering angle δ_{steer}, longitudinal velocity $\dot{x}$, lateral acceleration a_y, and yaw angle ω_z are used to obtain the estimated sideslip angle $\hat{\beta}_1$, compare Figure 6. (O1) includes a Luenberger observer that uses estimates and measurements of a_y and ω_z as feedback to steer the front and rear axles to optimally match the measured data. The rear axle is either steered in the same direction to match the lateral acceleration Figure (5 orange line) or steered to the opposite direction to match the yaw velocity Figure (5 blue line).

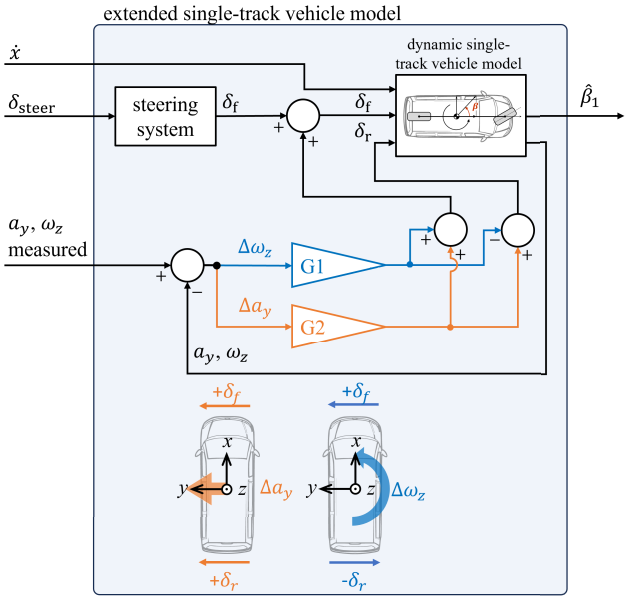

FIGURE 5. Model-based observer (O1).

ARTIFICIAL NEURAL NETWORK (O2)

The data-driven observer design (O2) depicted in Figure 7 is solely composed of an artificial neural network which considers the whole vehicle as a black box without any knowledge regarding the physical vehicle parameters or configuration.

The ANN is designed in MATLAB 2024b [30] using the corresponding Deep Learning Toolbox [31]. The network

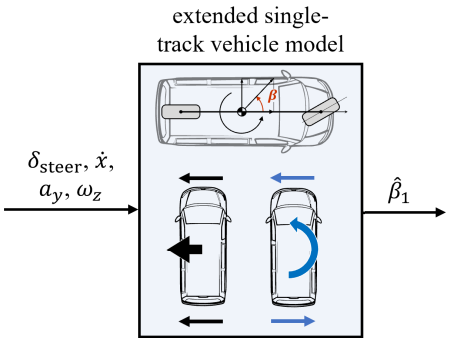

FIGURE 6. Simplified representation of (O1), compare Figure 5.

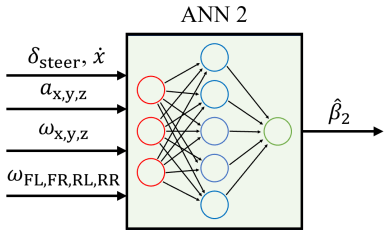

FIGURE 7. Data-driven observer (O2).

architecture comprises an input layer consisting of 12 neurons, a fully connected hidden layer consisting of 24 neurons that utilize either Long Short-Term Memory (LSTM) or Gated Recurrent Unit (GRU) cells, and an output layer consisting of one neuron. The input vector/set connecting to the input layer of the ANN is selected similarly to [5], [12], [13], and [15] as

$$u_{\text{ANN}} = \left[\delta_{\text{steer}}, \dot{x}, a_x, a_y, a_z, \omega_x, \omega_y, \omega_z, \ldots \right. \\ \left. \omega_{\text{fl}}, \omega_{\text{fr}}, \omega_{\text{rl}}, \omega_{\text{rr}}\right]^{\text{T}}, \tag{7}$$

while the hidden LSTM/GRU layer has twice the number of units in the sequence input layer. The output layer contains a single neuron that represents the estimated sideslip angle $\hat{\beta}_2$.

To optimally adapt learning rates during the training process, the Adaptive Moment Estimation (ADAM) algorithm was chosen similarly to [15], [16], [18], and [19]. In contrast to ADAM, other explored optimization methods, including Stochastic Gradient Descent with momentum (SGDM), Root mean square propagation (RMSprop), and Broyden–Fletcher–Goldfarb–Shanno (BFGS), failed to achieve comparable convergence rates or final performance.

A sigmoid function was used for gate activation. For the state activation, both hyperbolic tangent (tanh) and rectified linear unit (ReLU) functions were investigated, with the hyperbolic tangent used in the final configuration.

PHYSICS-INFORMED ANN (O3)

The physics-informed ANN (O3) depicted in Figure 8 combines the model-based approach (O1) with the data-driven approach (O2) in that the output of the single-track vehicle model guides the ANN (O2), which is extended by the respective additional input of $\hat{\beta}_1$ (resulting in the new artificial network ANN3). The network ANN3 then subsequently estimates the final sideslip angle $\hat{\beta}_3$ as depicted in Figure 8. The network architecture comprises an input layer consisting of 13 neurons, a fully connected hidden layer consisting of 26 neurons that utilize either LSTM or GRU cells, and an output layer consisting of one neuron.

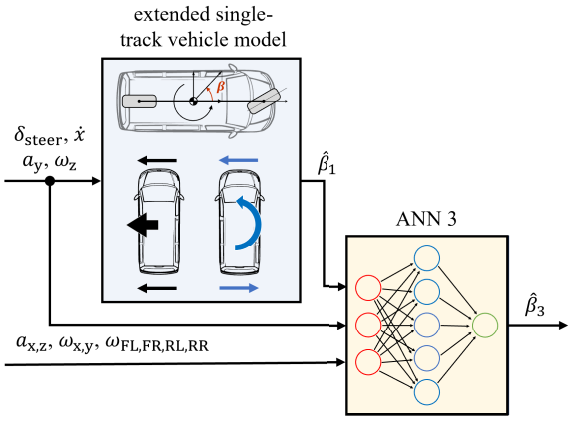

FIGURE 8. Physics-informed ANN (O3).

The performance of the physics-informed ANN is found to be highly sensitive to the training dataset used. The distribution of the measured sideslip angle within the training data significantly influences accuracy. The most accurate results are obtained for sideslip angles up to 1°, typical β-values that are overrepresented in the utilized training data.

PHYSICS-INFUSED ANN (O4)

In contrast to (O3), the physics-infused ANN (O4) depicted in Figure 9 operates on the principle that the physical model (O1) directly calculates $\hat{\beta}_1$, with the ANN4 subsequently estimating only the deviation from the reference signal $\hat{\beta}_1$. In an input layer the ANN is presented with a signal from the extended single-track vehicle model (O1) $\hat{\beta}_1$ and is estimating the error of the physical model $\Delta\hat{\beta}$ and the final estimate is calculated as $\hat{\beta}_4 = \Delta\hat{\beta} + \hat{\beta}_1$.

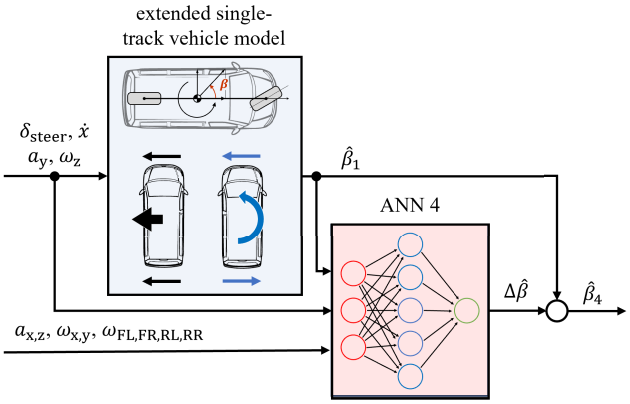

FIGURE 9. Physics-infused ANN (O4).

ANN4 is trained using the sideslip angle estimated/measured by the expensive IMU as a reference signal. The network architecture is composed of an input layer containing 13 neurons, a fully connected hidden layer of 26 neurons, LSTM or GRU cells, and an output layer with one neuron.

(O4) exhibits worse performance at small sideslip angles when compared to (O3). Conversely, (O4) design maintains a nearly constant accuracy across its entire operating range, which also extends beyond the working area of (O3) design. It is important to note that the output layer or the reference represents $\Delta\hat{\beta} = \beta_{\text{measured}} - \hat{\beta}_1$, rather than the $\hat{\beta}$ quantity directly.

HYBRID ANN MODEL STRUCTURE (O5)

While the physics-informed design (O3) demonstrates satisfactory performance, its effectiveness is primarily limited to scenarios involving small values of β. In contrast, the physics-infused design (O4) offers relatively stable performance across a wider operating range. This observation motivates a selective strategy, wherein each design is applied within the regime where it performs best.

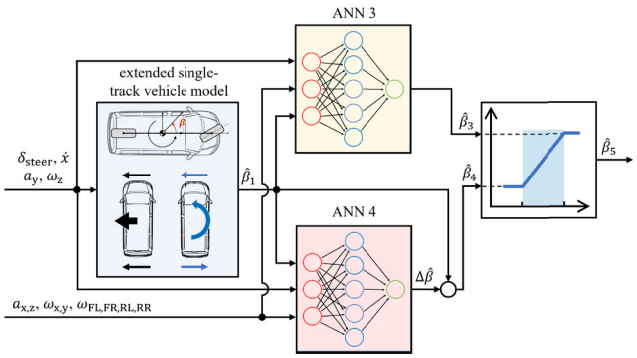

FIGURE 10. Hybrid ANN observer design (O5) with output selection and weighting detailed in Figure 11.

To implement this strategy, a combined design (O5) depicted in Figure 10 is developed, leveraging the strengths of both approaches (O3) and (O4) based on the predicted value of $\hat{\beta}_4$ from the physics-infused design. Specifically, the hybrid design (O5) operates as the physics-informed design (O3) for $\hat{\beta}_4 \leq 1°$, and switches to the physics-infused design (O4) for $\hat{\beta}_4 \geq 2°$. In the transition interval between 1° and 2°, the estimation is computed as a weighted sum of both designs, with the weighting determined by the output of the physics-infused design. This approach is illustrated in Figure 11 and Figure 12. Estimate $\hat{\beta}_4$ is used for switching respective weighting between $\hat{\beta}_3$ and $\hat{\beta}_4$ because the physics-infused design provides a consistently accurate estimate of β over the whole operation range (while providing slightly worse accuracy compared to (O3) for small sideslip angles).

IV. RESULTS AND DISCUSSION

This section presents the results of the sideslip angle estimation using the observer designs (O1) to (O5) described in

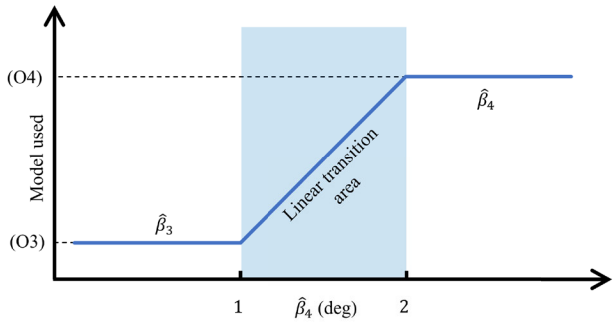

FIGURE 11. Output selection and weighting of hybrid ANN observer design (O5).

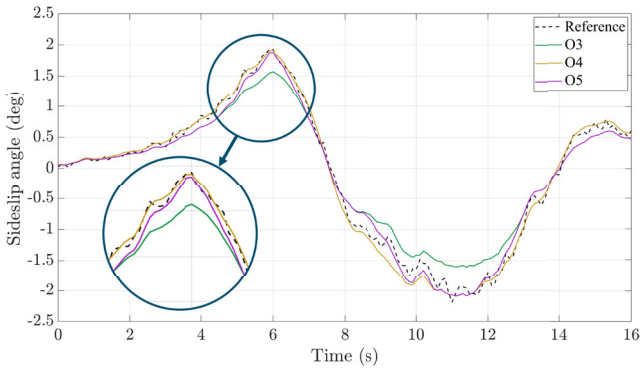

FIGURE 12. Reference vs. estimated values of β for the design architectures (O3) to (O5) for validation data from tire sets 2. The design architectures utilize a LSTM network. The transition of the hybrid structure design (O5) between $\hat{\beta}_3$ and $\hat{\beta}_4$ for $1° \leq \beta \leq 2°$ is highlighted.

Section III, evaluated on the dataset detailed in Section II-D. Prior to training and evaluation, the cornering stiffness coefficient of each tire was integrated into the Simulink model and model-based observer (O1). The Root Mean Squared Error (RMSE) was employed as the Key Performance Indicator (KPI):

$$RMSE = \sqrt{\sum_{i=1}^{n} \frac{(\hat{\beta}_i - \beta_i)^2}{n}}, \tag{8}$$

where $\hat{\beta}_i$ represents the estimated and β_i the measured reference (ground truth) sideslip angle, and n is the number of samples.

A. PROOF OF CONCEPT USING A HIGH-QUALITY IMU

For a proof-of-concept study, the signals (7) were initially acquired using a high-fidelity IMU. Two distinct ANN architectures, LSTM and GRU networks, were subsequently evaluated for sideslip angle estimation. They showed similar performance, see Table 3 for their RMSE performance. We analyze the LSTM-based results in detail in Figure 14 and Figure 15.

The data-driven black-box observer design (O2), visually represented in Figure 14 and Figure 15 in red, exhibited a high

TABLE 3. RMSE of observer designs (O1) - (O5) using LSTM/GRU architectures and data obtained by a high-quality IMU.

	Training	Validation	Test I.	Test II.	Test III.
			Vehicle observer		
O1	0.1491°	0.1281°	0.0988°	0.0989°	0.1102°
			LSTM		
O2	0.1302°	0.0852°	0.1077°	0.0921°	0.1314°
O3	0.1177°	0.0749°	0.0942°	0.0765°	0.0751°
O4	0.0632°	0.0612°	0.0729°	0.0806°	0.0743°
O5	0.0709°	0.0639°	0.0589°	0.0669°	0.0642°
			GRU		
O2	0.1207°	0.0819°	0.1033°	0.0972°	0.1274°
O3	0.1056°	0.0693°	0.0795°	0.0720°	0.0681°
O4	0.0648°	0.0607°	0.0644°	0.0725°	0.0649°
O5	0.0717°	0.0640°	0.0575°	0.0639°	0.0640°

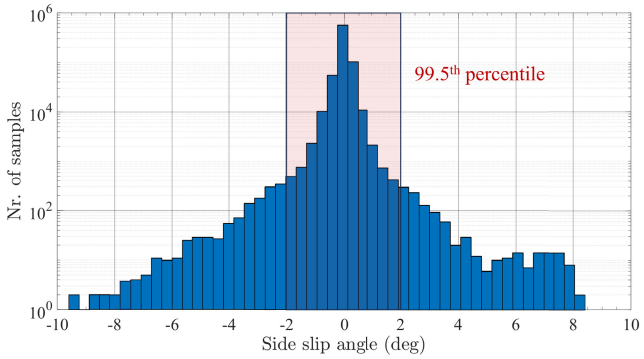

FIGURE 13. Combined sideslip angle distribution of all measurement datasets. The y-axis is scaled logarithmically for better visualization. Sideslip values exceeding 2° constitute less than 0.5 % of all collected samples.

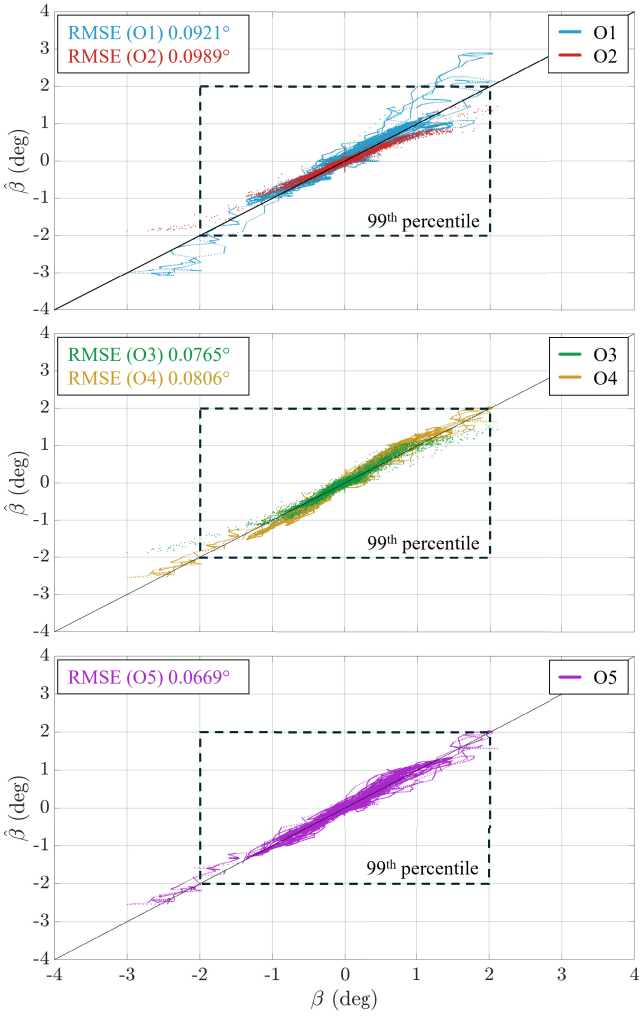

FIGURE 14. Reference vs. estimated values of β for (O1) to (O5) tested on the testing set II. The observer designs (O2) to (O5) utilize an LSTM network.

degree of accuracy in the estimation of small sideslip angle values, specifically those not exceeding 1°. This observation aligns precisely with the findings in [32], which indicate that data-driven methodologies generally show good performance within their training range. Nevertheless, a degradation in the performance of the data-driven design was observed beyond sideslip angle magnitudes $|\beta|$ of 2°. In contrast to (O2), the model-based observer design (O1), depicted in Figure 14 and Figure 15 in blue, showed decreased performance in the estimation of small β values. Despite this, (O1) demonstrably surpassed (O2) in performance when the sideslip angle β exceeded 1.5°. However, the performance of (O1) is limited by the use of a linear tire model, whose accuracy decreases significantly as the static characteristics of the tire force become more saturated. On the other hand, the use of (O2) is limited by the sparsity of the data sets in the high sideslip range. Examining the two hybrid designs, the physics-informed (O3) and physics-infused (O4) approaches consistently outperformed the purely model-based and purely data-driven observer designs (O1 and O2), as shown in Table 3. It should be mentioned that investigating both the timeseries results and Table 3 the performance of both (O3) and (O4) directly depend on the training dataset. In most of the cases (O3), visually represented in Figure 14 in green, performed with greater accuracy in situations involving small sideslip angles (approximately below 1°). However, when the dataset incorporated β values exceeding 1.5°, (O4) consistently exhibited better performance compared to (O3). This is due to the more significant role of the model-based observer (within the (O4) design compared to the (O3) design), particularly in the estimation of β, when it is not sufficiently represented in the training dataset.

Although high β scenarios represent a minority of driving situations, they cannot be completely ignored. Therefore, a hybrid structure (O5) was developed to combine the accuracy of the data-driven design at small sideslip angles with the robustness of the model-based observer at larger sideslip angles. Design (O4), while less accurate, provides a robust general estimate of β values. Therefore, in the hybrid structure (O5), the parameter $\hat{\beta}_4$ is chosen as a critical determinant of the observer's behavior. Specifically, the design transitions between two operational modes based on the value of $\hat{\beta}_4$:

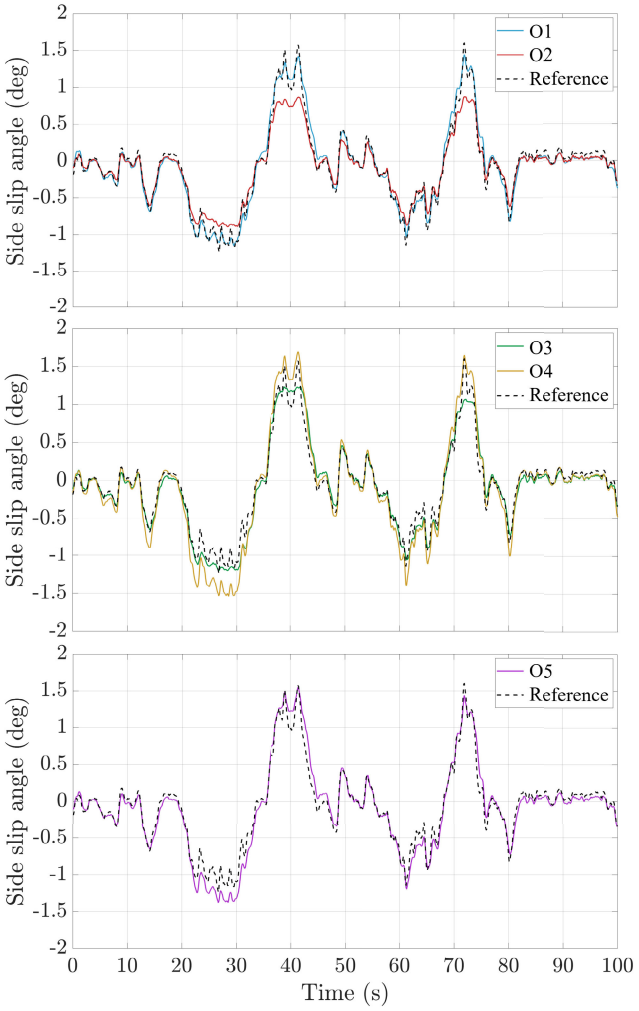

FIGURE 15. Time series data of β and $\hat{\beta}$ for a selected portion of the testing set II. The observer designs (O2) to (O5) utilize an LSTM network.

- $|\hat{\beta}_4| \leq 1°$: The design adopts the physics-informed structure (O3). In this mode, the design integrates physical knowledge while allowing for greater flexibility, through data-driven ANN, to complement or enhance the physics-based elements of (O1).
- $|\hat{\beta}_4| \geq 2°$: The design shifts to the physics-infused structure (O4). Here, the design is predominantly constrained by physical laws.
- $1° < |\hat{\beta}_4| < 2°$: In the transition region, the design's output is a weighted sum of the physics-informed and physics-infused design outputs, with weights linearly adjusted based on $\hat{\beta}_4$.

The results demonstrate that (O5) shows better performance compared to all of the previous designs (O1) - (O4) across most of the evaluated scenarios. This is quantitatively supported by the data presented in Table 3 and visually corroborated by Figure 16. The performance of (O5) was matched by other designs only in Test III, specifically when utilizing the GRU ANN, where its improvement over (O4) was marginal. This can be attributed to (O5) operating predominantly as (O4) in this particular scenario. Notably (O4) and (O5) demonstrated a consistently high fit. This robust performance was sustained even in rare, high β scenarios, while the fit of (O2) and (O3) exhibited a rapid deterioration for $|\beta| > 2°$. It is important to note that the majority of the collected data (99.5 %) correspond to sideslip angles $|\beta| < 2°$, with only 0.5 % of the data falling into the higher β range, compare Figure 13.

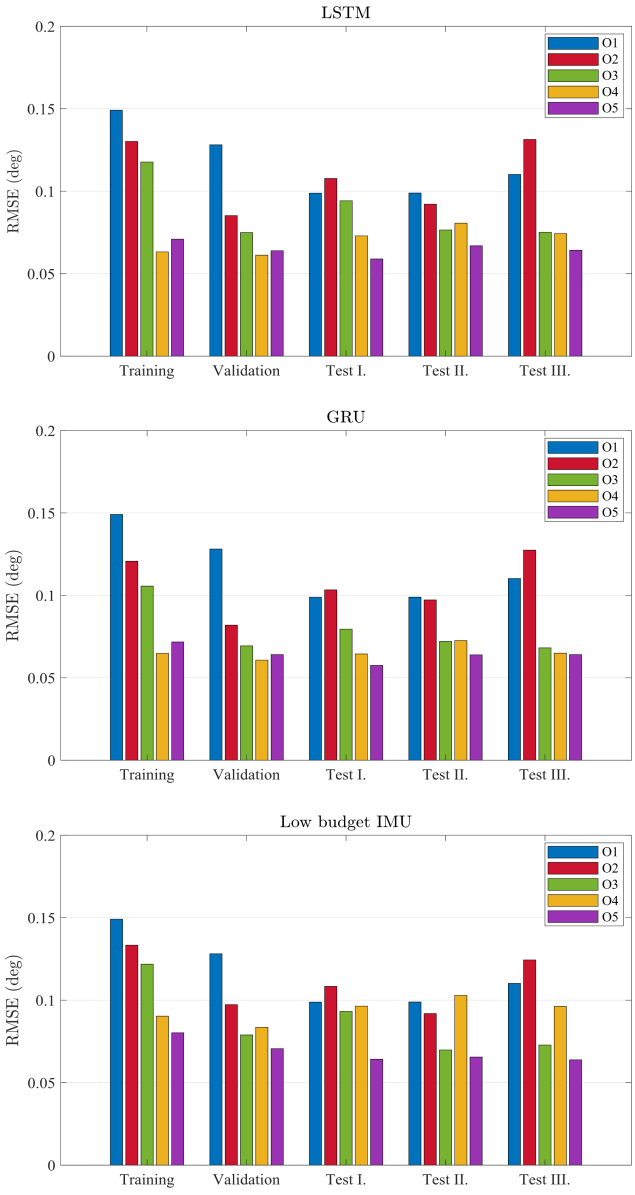

FIGURE 16. RMSE of the vehicle sideslip angle estimation.

B. VALIDATION USING A LOW-BUDGET IMU

To validate this proof of concept, the trained ANNs were fed with data from a low-budget IMU. The assessments in the Section IV-A revealed very similar results between the LSTM and GRU networks. Consequently, we selected only

the LSTM network to evaluate the preliminary viability of our proposed methodology. The results are then shown in Table 4 and visually corroborated by Figure 16. A more detailed investigation is planned as part of future research.

TABLE 4. RMSE of observer designs (O1) - (O5) using LSTM architectures and data obtained by a low-budget IMU.

	Training	Validation	Test I.	Test II.	Test III.
			Vehicle observer		
O1	0.1491°	0.1281°	0.0988°	0.0989°	0.1102°
			LSTM Low budget IMU		
O2	0.1333°	0.0973°	0.1084°	0.0919°	0.1244°
O3	0.1218°	0.0789°	0.0932°	0.0698°	0.0728°
O4	0.0903°	0.0836°	0.0964°	0.1029°	0.0962°
O5	0.0802°	0.0706°	0.0642°	0.0655°	0.0638°

C. DATA AVAILABILITY

The acquisition of real-vehicle test data encompassing highly varying β values presents inherent challenges, as extensively documented within academic discourse, notably in [15] and [19]. Prior investigations frequently employed high-performance rear-wheel drive vehicles, which are inherently more susceptible to oversteer and possess the inherent capability to sustain larger β values. In stark contrast, the front-wheel drive vehicle, the characteristics of which are detailed in Section II-B, rarely exhibits such dynamic states, thereby imposing a significant limitation upon the availability of substantial β data within the training dataset. An analysis of the β distribution within the dataset, visually represented by a histogram comprising 50 bins in Figure 13, revealed that instances of β values exceeding 2° are exceedingly rare, constituting less than 0.5 % of all collected samples. It was verified that the training, validation, and testing datasets showed consistent distributions.

V. CONCLUSION

This study demonstrated that purely data-driven methods for estimating the sideslip angle β are highly sensitive to the training dataset, limiting their ability to provide robust estimates of β under extreme driving conditions. We showed that combining data-driven and model-based approaches provides a promising way to overcome these limitations of sparse but representative training datasets, particularly with respect to their performance in edge cases. By integrating a data-driven estimator into a model-based framework, robust performance can be maintained under typical driving conditions, while the model-based component effectively supports estimation in edge cases. Importantly, increasing design complexity does not necessarily improve accuracy. Instead, the complementary strengths of data-driven and model-based methods can be leveraged through their combination. The datasets used in this work were measured under real-world conditions using five different tire sets, and the proposed observer designs were validated accordingly. The presented hybrid ANN observer design (O5) enables sideslip angle estimation using artificial neural networks in combination with a model-based approach. This directly addresses the research question, confirming that reliable estimation of β is feasible using hybrid methods trained on data from typical, rather than extreme, driving scenarios. In conclusion, this study highlights the potential of hybrid estimators that combine physics-based observers with ANN techniques for vehicle state estimation, specifically for sideslip angle estimation. Fleet tests with low-cost IMUs and data-logging capabilities facilitate large-scale validation across multiple vehicles, providing detailed insights into tire–road interactions.

Future research should examine the influence of additional key performance indicators (KPIs) and further investigate how hardware requirements, training time, and computational load affect overall system performance.

REFERENCES

[1] A. L. Gratzer, M. M. Broger, A. Schirrer, and S. Jakubek, "Two-layer MPC architecture for efficient mixed-integer-informed obstacle avoidance in real-time," *IEEE Trans. Intell. Transp. Syst.*, vol. 25, no. 10, pp. 13767–13784, Oct. 2024.
[2] A. L. Gratzer, A. Schmiedhofer, A. Schirrer, and S. Jakubek, "Agile mixed-integer-based lane-change MPC for collision-free and efficient autonomous driving," *IEEE Trans. Intell. Vehicles*, early access, Oct. 7, 2024, doi: 10.1109/TIV.2024.3476423.
[3] X. Li, X. Song, and C. Chan, "Reliable vehicle sideslip angle fusion estimation using low-cost sensors," *Measurement*, vol. 51, pp. 241–258, May 2014.
[4] M. Tristano, B. Lenzo, H. Saxton, X. Xu, and X. Zhang, "Physics-infused neural network-driven investigation of vehicle sideslip angle," in *Advances in Dynamics of Vehicles on Roads and Tracks III*, W. Huang and M. Ahmadian, Eds., Cham, Switzerland: Springer, 2024, pp. 358–365.
[5] J. Liu, Z. Wang, L. Zhang, and P. Walker, "Sideslip angle estimation of ground vehicles: A comparative study," *IET Control Theory Appl.*, vol. 14, no. 20, pp. 3490–3505, Dec. 2020.
[6] A. H. Salari, H. Mirzaeinejad, and M. F. Mahani, "Tire normal force estimation using artificial neural networks and fuzzy classifiers: Experimental validation," *Appl. Soft Comput.*, vol. 132, Jan. 2023, Art. no. 109835.
[7] S. Melzi and E. Sabbioni, "On the vehicle sideslip angle estimation through neural networks: Numerical and experimental results," *Mech. Syst. Signal Process.*, vol. 25, no. 6, pp. 2005–2019, Aug. 2011.
[8] T. Novi, R. Capitani, and C. Annicchiarico, "An integrated artificial neural network–unscented Kalman filter vehicle sideslip angle estimation based on inertial measurement unit measurements," *Proc. Inst. Mech. Engineers*, vol. 233, no. 7, pp. 1864–1878, 2018.
[9] M. Kato, "Estimation of vehicle side slip angle with artificial neural network," *JSAE Rev.*, vol. 15, no. 1, pp. 79–81, Jan. 1994.
[10] D. Fényes, B. Németh, M. Asszonyi, and P. Gáspár, "Side-slip angle estimation of autonomous road vehicles based on big data analysis," in *Proc. 26th Medit. Conf. Control Autom. (MED)*, Jun. 2018, pp. 849–854.
[11] H. Sasaki and T. Nishimaki, "A side-slip angle estimation using neural network for a wheeled vehicle," *SAE Trans.*, vol. 109, pp. 1026–1031, Mar. 2000.
[12] X. Du, H. Sun, K. Qian, Y. Li, and L. Lu, "A prediction model for vehicle sideslip angle based on neural network," in *Proc. 2nd IEEE Int. Conf. Inf. Financial Eng.*, Sep. 2010, pp. 451–455.
[13] D. Chindamo and M. Gadola, "Estimation of vehicle side-slip angle using an artificial neural network," in *Proc. MATEC Web Conferences*, vol. 166, 2018, p. 02001.
[14] *Introduction to CarSim*, MS Corporation, Ann Arbor, MI, USA, 2021.
[15] T. Gräber, S. Lupberger, M. Unterreiner, and D. Schramm, "A hybrid approach to side-slip angle estimation with recurrent neural networks and kinematic vehicle models," *IEEE Trans. Intell. Vehicles*, vol. 4, no. 1, pp. 39–47, Mar. 2019.
[16] P. M. Sieberg, S. Blume, and D. Schramm, "Side-slip angle estimation by artificial neural networks for vehicle dynamics control applications," in *Proc. AmE-Automot. Meets Electron., 12th GMM-Symp.*, Mar. 2021, pp. 1–6.

[17] P. M. Sieberg, S. Blume, S. Reicherts, N. Maas, and D. Schramm, "Hybrid state estimation—A contribution towards reliability enhancement of artificial neural network estimators," *IEEE Trans. Intell. Transp. Syst.*, vol. 23, no. 7, pp. 6337–6346, Jul. 2022.
[18] M. G. Essa, C. M. Elias, and O. M. Shehata, "Comprehensive performance assessment of various NN-based side-slip angle estimators (ANN-SSE)," in *Proc. IEEE 93rd Veh. Technol. Conf. (VTC-Spring)*, Apr. 2021, pp. 1–6.
[19] A. Bertipaglia, M. Alirezaei, R. Happee, and B. Shyrokau, "An unscented Kalman filter-informed neural network for vehicle sideslip angle estimation," *IEEE Trans. Veh. Technol.*, vol. 73, no. 9, pp. 12731–12746, Sep. 2024.
[20] *Road Vehicles - Vehicle Dynamics Test Methods-Part 1: General Conditions for Passenger Cars*, Standard ISO 15037-1:2019, Mar. 2019.
[21] *GeneSys Datasheet ADMA-G-Pro+*, GeneSys Elektronik GmbH, Offenburg, Germany, 2001.
[22] *Road Vehicles-Vehicle Dynamics and Road-holding Ability-Vocabulary*, Standard ISO 8855:2011, 2011.
[23] T. D. Gillespie, *Fundamentals of Vehicle Dynamics*. Warrendale, PA, USA: SAE, 1992.
[24] W. F. Milliken, D. L. Milliken, and L. D. Metz, *Race Car Vehicle Dynamics*. Warrendale, PA, USA: SAE, 1995.
[25] *Vehicle Dynamics Blockset™ Reference*, The MathWorks Inc., Natick, MA, USA, 2024.
[26] D. Schramm, M. Hiller, and R. Bardini, *Vehicle Dynamics: Modeling and Simulation*, 2nd ed., Cham, Switzerland: Springer, 2018.
[27] D. Vetturi, A. Magalini, and M. Gadola, "Use of an innovative multi-input one-output lfn network for experimental data numerical description," in *Proc. TMT-7th Int. Res./Expert Conf. Trends Develop. Machinery*, 2003.
[28] M. T. Hagan, H. B. Demuth, and M. Beale, *Neural Network Design*. Boston, MA, USA: PWS Publishing, 1997.
[29] *Simulink Reference*, The MathWorks Inc., Natick, MA, USA, 2024.
[30] *MATLAB Version*, The MathWorks Inc., Natick, MA, USA, 2024.
[31] *Deep Learning Toolbox™ User's Guide*, The MathWorks Inc., Natick, MA, USA, 2024.
[32] A. Bertipaglia, "Control of evasive manoeuvres for automated driving," Ph.D. dissertation, Dept. Cogn. Robot., Delft Univ. Technol., The Netherlands, 2025.

MARTIN REPKA received the M.Sc. degree in mechanical engineering from Brno University of Technology, Brno, Czech Republic, in 2021. He is currently pursuing the Ph.D. degree. Since 2021, he has been a member of the Project Team, Institute of Automotive Engineering, Brno University of Technology. His research interests include modeling, multi-body systems, and observers, with a recent focus on machine learning-based estimators.

ALEXANDER L. GRATZER (Member, IEEE) received the M.Sc. and Ph.D. degrees in mechanical engineering from TU Wien, Vienna, Austria, in 2019 and 2025, respectively. Since 2019, he has been a member of the Project Team, Institute of Mechanics and Mechatronics, TU Wien. His research interests include modeling, control, and optimization of complex systems, with a recent focus on automated driving and intelligent transportation systems (ITS).

JAN FOJTASEK received the M.Sc. and Ph.D. degrees in mechanical engineering from Brno University of Technology, Brno, Czech Republic, in 2014 and 2020, respectively. Since 2020, he has been a Postdoctoral Researcher and a Teacher with the Institute of Automotive Engineering, Brno University of Technology. His research interests include vehicle dynamics modeling, real world testing, and multi-body systems and simulations.

TOMAS STRAKA received the M.Sc. degree in mechanical engineering from Brno University of Technology, Czech Republic, in 2021. He is currently pursuing the Ph.D. degree. Since 2021, he has been a member of the Project Team, Institute of Automotive Engineering, Brno University of Technology. His research interests include tire mechanics, magic formula tire models, and the automated analysis of road measurement data.

PETR PORTES received the M.Sc., Ph.D., and Habilitation degrees in mechanical engineering from Brno University of Technology, Czech Republic, in 1988, 1997, and 2015, respectively. Since 2014, he has been leading the Sub Department of Motor Vehicles at the Institute of Automotive Engineering, Brno University of Technology. He was a Senior Lecturer with the Institute of Automotive Engineering, Brno University of Technology. His research interests include vehicle dynamics, with a particular emphasis on computational modeling, experimental validation, and applications within motorsport.

ALEXANDER SCHIRRER received the M.Sc., Ph.D., and Habilitation degrees in mechanical engineering from TU Wien, Vienna, Austria, in 2007, 2011, and 2018, respectively. Since 2011, he has been a Postdoctoral Researcher and a Teacher of graduate-level lectures with the Institute of Mechanics and Mechatronics, TU Wien. His research interests include modeling, simulation, optimization, and control of complex and distributed-parameter systems.